Geologic implications of aeromagnetic data over the volcanic plateau, Western Yemen

Amin Noman Al Kadasi
Department of Geology, Faculty of Applied science, Taiz University, Taiz, Yemen
E-mail address: alkadasi2000@yahoo.com

ABSTRACT

Aeromagnetic data of the study area was reduced to the pole (RTP), spectrally analyzed, and separated into regional and local magnetic anomaly sets. These sets of magnetic anomalies are carefully analyzed and the gross structural pattern of the area is derived from the interpreted major faults and integrated boundaries of the RTP and regional anomalies. The regional trends in the area are terminated in the eastern part by N-S trending narrow basins developed by escape blocks tectonism beneath the Dhamar – Rada'a Quaternary volcanic field and the Damt geothermal site, associated with the collision of east and west Gondwana. This may explain the fumaroles at the Al Lisi active volcano and the highest mantle imprint of gases emitted at the Damt geothermal site, compared with the other geothermal fields in Yemen. The volcanic activity in this volcanic field mostly also originated by reactivating these deeper structures.

The major faults interpreted from magnetic anomalies are exactly match, in the study area, the regional faults extended from the Paleozoic Sana'a basin which may suggests that this basin is extended through the Yemeni highlands (below the Cenozoic volcanic and Mesozoic lithology) from the north of Sana'a to the area of study.

Repeated reactivation of Precambrian structures creates nets of interconnected deep faults in the area which assist the partial melting of the mantle and resulted in the widespread magmatic intrusion invaded the area, as well as in the observed geothermal activity.

KEYWORDS: Aeromagnetic, Magnetic anomaly, Geologic structures, Edge detector filters, Arabian shield, Magmatic intrusion.

INTRODUCTION

Geophysical studies are generally aimed to carefully image the geologic and tectonic framework of investigated regions. Magnetic survey data is routinely used in delineating subsurface geologic structures by analyzing magnetic anomalies and tracing the contact between the different lithologic units, based on the lateral variation in magnetic susceptibility. A wide range of signal enhancement techniques has been developed for mapping magnetic contact based initially on calculating the vertical and horizontal derivatives of the magnetic field and classified into two classes (e.g. Pilkington and Keating 2004; Cooper and Cowan 2008; Cooper 2009; Arisoy and Dikmen 2013; Ma et al. 2014). The first class exhibits maxima over magnetic contacts (e.g. total horizontal derivative and enhanced total horizontal derivative of the tilt angle). In the second class, magnetic contacts are defined by the zero contour which marks the transition of magnetic polarity from positive to negative (e.g. vertical derivative and tilt angle derivative). Due to the drawback associated with edge detector techniques (Pilkington and Keating 2004; Cooper 2009; Arisoy and Dikmen 2013) a confident picture of the subsurface can be obtained by integrating the results of several techniques.

In this study, aeromagnetic data were reduced to the pole, spectrally analyzed and separated

into local and regional anomalies. Then the data are carefully analyzed and subjected to seven edge detector techniques (vertical derivative VDR, total horizontal derivative THD, tilt angle derivative TDR, horizontal tilt angle TDX, Etilt, enhanced total horizontal derivative of the tilt angle ETHDR, and theta map)and Euler deconvolution in an attempt to understand the geologic and tectonic setting of the study area which offers important background for natural resources investigation (e.g. geothermal energy, minerals, groundwater, .. etc) and environmental studies. The area of study is located in the western part of Yemen bounded by latitudes 14^{o} – 15^{o} N and longitudes 43.5^{o} – 45^{o} E and covered mostly by the Cenozoic volcanics in addition to the Precambrian basements and scattered exposures of the Mesozoic sedimentary rocks (Fig. 1).

GEOLOGIC AND TECTONIC SETTING

The geology of Yemen is founded by the Arabian shield which originated during the Pan-African Orogeny, about 750 – 600 Ma (million years ago), by the accretion of low-grade island-arc terranes and high-grade continental terranes (Stoeser and Camp 1985; Blasband et al. 2000). The final stage of the Pan-African Orogeny leads to the development of the Najd fault system which is characterized by large shear zones and NW – SE trending strike-slip faults (Levin and Park 2000; Nehlig et al. 2002). The basement rocks in Yemen, located in the southern part of the Arabian shield, divided into six terranes, four gneissic (Asir, Afif, Abas, and Al Mahfidterranes) and two island arcs (Al Bayda and Al Mukallaterranes). The basement tectonics in Yemen is oriented mainly N–S, NW–SE, NE–SW and subordinately E–W (As-Saruri et al. 2010).

The basement rocks in the study area belong to the Abasterrane (Fig. 2) and mostly exposed in the eastern part of the area at the upper eastern corner and along the eastern boundary. In the western part of the area, they are occurred in the form of small elongated exposures. These rocks include mainly migmatite, paragneiss, schist, metavolcanics, quartzite, amphibolites, marble, metadolomite, syntectonic to posttectonic granite and diorite (Fig. 1).

The breakup of Gondwana and the separation of India – Madagascar from the Afro – Arabia during the Late Jurassic - Early Cretaceous reactivated the Najd fault system and resulted in the development of several subparallel extensional basins trending NW-SE in the western part of Yemen (Fig. 2) to WNW-ESE and W-E in the eastern part. The local fault events within the Mesozoic basins give rise to the formation of sub-basins, half-grabens and intra-basinal horst structures which are largely influenced the thickness of sedimentary rocks (Beydoun et al. 1996 and 1998). The WadiSiham-Ad Dali' basin (Fig. 2) is one of the Mesozoic basins which extended from the passive margin of the Gulf of Aden in the south to the Tihamah plain in the west and cutting obliquely through the study area between the southern and western boundaries. This basin reactivated during the Late Oligocene - Miocene rifting, associated with the separation of Arabia from Africa, and covered by a thick blanket of volcanic rocks, Yemen trap series YTS.

The sedimentary rocks in the area of study represented by Jurassic limestone (Amran Group) and Cretaceous sandstone (Tawilah Group). These rocks are heavily faulted and occurred in the form of an irregular strip separated the volcanic plateau from the Precambrian basement in the eastern part of the area. They also occur in the form of elongated patches in the western

part of the area (Fig. 1).

The Tertiary volcanic activity in Yemen, which is related to the impact of the Afar mantle plume, resulted in a thick sequence of the Yemen trap series (YTS) covering about 50000 km^2 in the western part of Yemen known as the volcanic plateau or the plateau (Yemeni highlands). The YTS, lower part of the Yemen Volcanic Group "YVG", emplaced during the Oligo-Miocene and characterized by two distinct events. "YVG", emplaced during the Oligo-Miocene and characterized by two distinct events. The first

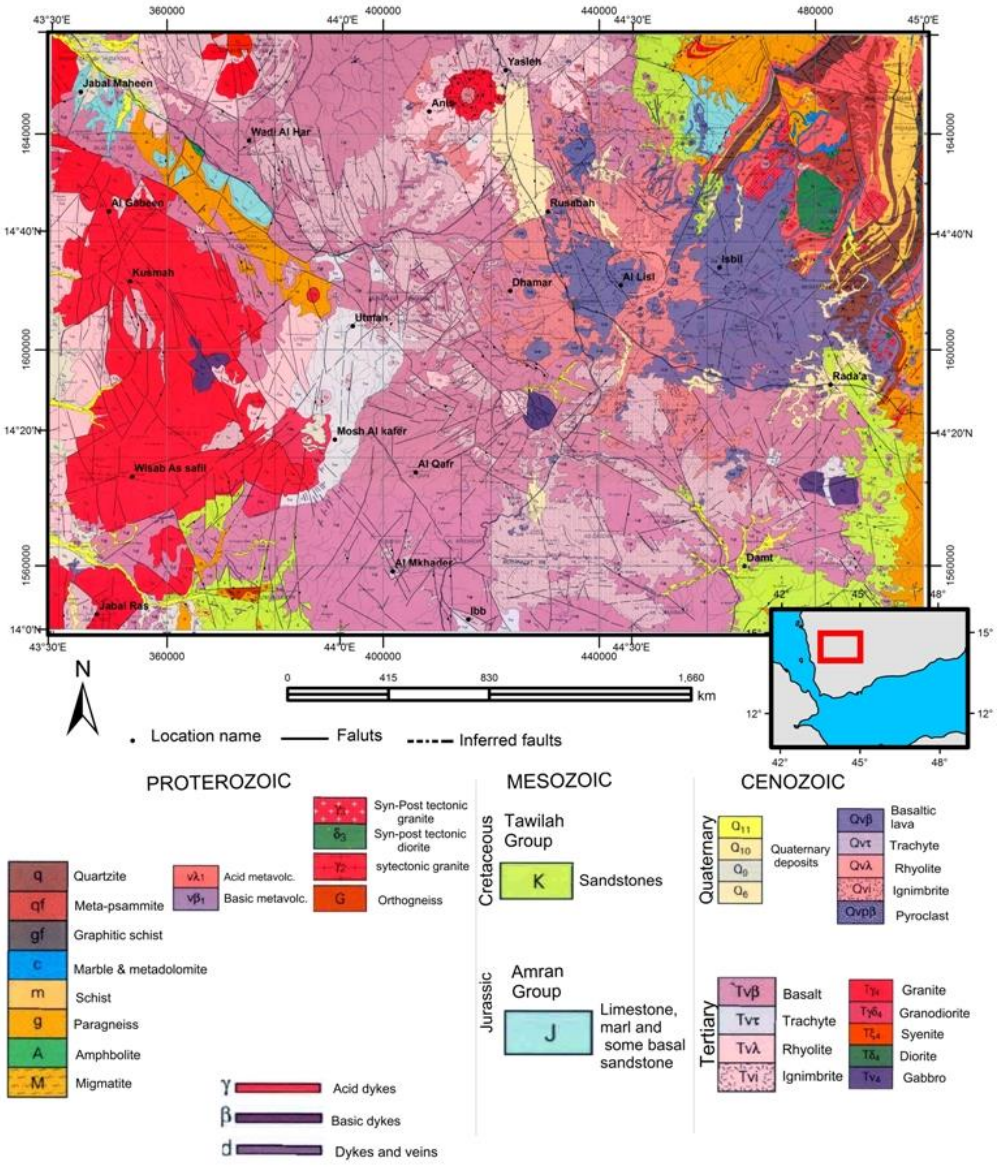

Fig. 1 Location and geological map of the study area (Adapted from Robertson 1990)

event, 30 – 26 Ma, characterized by lava flows erupted throughout the whole plateau along N-S trending fissures and composed mainly of basalt, rhyolite, ignimbrite and volcanic glass. The second event, emplaced between 22 – 19 Ma, is dominated in the southern part of the plateau, and characterized by intrusive bodies (e.g. plugs, domes and dike swarms) of basalt, alkali-granites, syenite, and less frequently diorite and gabbro. The dike swarms trending

mostly NW-SE, NNW-SSE and concentrated mainly in the western part of the plateau (Chiesa et al. 1983; Huchon et al. 1991; Manetti et al. 1991; Davison et al. 1994). An intense phase of extension is heavily dissected the volcanic plateau, between 19 – 10 Ma, by NNW-SSE listric faults and NNE-SSW normal faults with sinistral strike-slip component (Chiesa et al. 1983; Huchon et al. 1991). In the southern part of Yemen, the YTS intruded by dike swarms trending mostly E-W to NE-SW (Moseley 1969). The largest part of the area of study is covered by the YTS.

The Quaternary volcanics constitute the Yemen Volcanic Series (YVS), the upper part of the YVG, which occurred in the form of strato-type volcanoes, cones, domes, sheets, and lava flows. In the study area, the

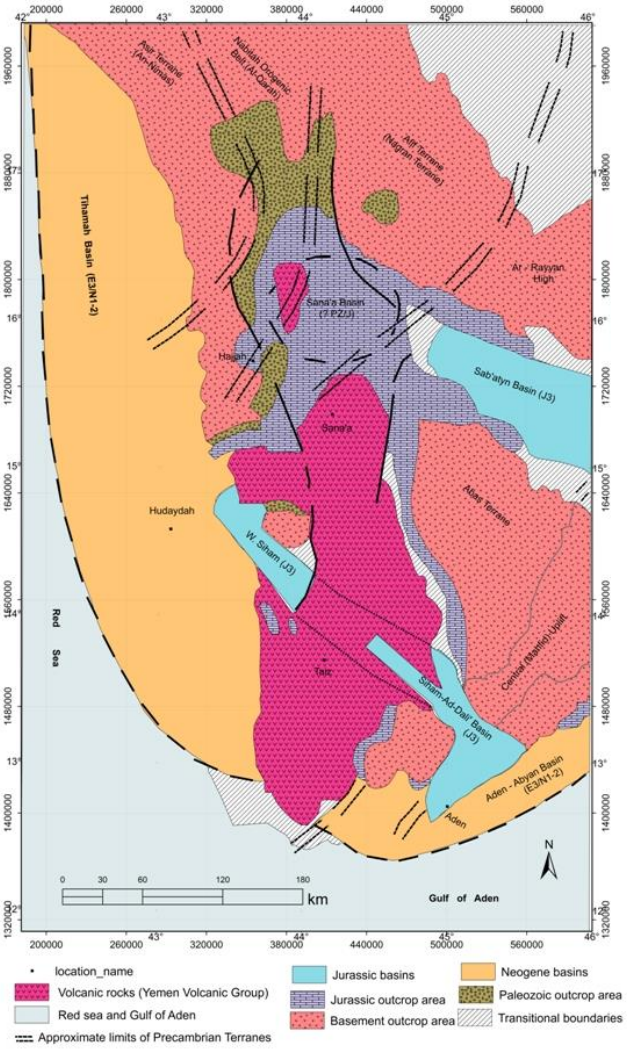

Fig. 2 The western part of the sedimentary basins map of Yemen (adapted from As-Saruri et al., 2010)

YVS is represented by the Dhamar – Rada'a Quaternary volcanic field at and around the eastern border of the volcanic plateau. This volcanic field is characterized by small horst and graben structures oriented mainly NNE-SSW and E-W (Chiesa et al. 1983). The early magmatic activity in this field was started about 6.4 – 5.7 Ma and composed mostly of ignimbrite and basaltic lava flows. The next activity, about 1.4-1.2 Ma, represented by the Al Lisi and Isbil active volcanoes and the final magmatic activity occurred since about 10 thousand years and characterized by fissure basalt flows and cinder cones (Manetti et al. 1991).

The youngest faults affected the volcanic plateau trending NE-SW, infrequently observed in the plateau, attributed to reactivation of the crystalline basement faults during the Late Tertiary - Quaternary (Manetti, et al. 1991).

AEROMAGNETIC DATA

The aeromagnetic map of Yemen, compiled by Robertson Group PLC in 1991 for the Yemeni ministry of oil and mineral resources, contains two sets of data. The first set is obtained by constant barometric altitude surveys and upward continued to 3350 m, while the second set is obtained by constant terrain clearance surveys and continued to 100 m. The survey lines in the study area oriented N 25^{o} E and separated by 1.5 – 2 km with a sampling interval of 40 m, while the tie lines oriented N 65^{o} W and separated by 5 – 10 km. The study area is enclosed by the aeromagnetic sheet 14G (scale of 1: 250000). It is mostly covered by a constant barometric survey except to a very limited portion at the southeastern corner of the area, bounded by a slash-dots black line (Fig. 3), which is covered by a constant terrain clearance survey. The data of this portion were separated, continued upward to 3350 m and remerged with the constant barometric data. Then the whole data gridded with a cell size of 400 m (one-fifth of the survey line spacing, to alleviate aliasing problem) and upward continued by a one-cell size to reduce the edge effect at the boundary between the two sets of data.

To accentuate magnetic anomalies directly above their sources and eliminate the shape distortion, assuming no remanent field, the data were reduced to the north magnetic pole by using the geomagnetic field parameters (inclination 14.28^{o}, declination 1.18^{o} and IGRF of 37692.5 nT) of the year 1985 at the center of the area (Robertson, 1991). The reduced to the pole (RTP) map of the study area (Fig. 3).

The 2D radially averaged power spectrum of the RTP data is calculated (Fig. 4) and the regional and local anomaly sets are separated from the RTP anomalies by using wave number bandwidths of 0.0145 - 0.070 km^{-1} and 0.070 - 0.266 km^{-1}, respectively.

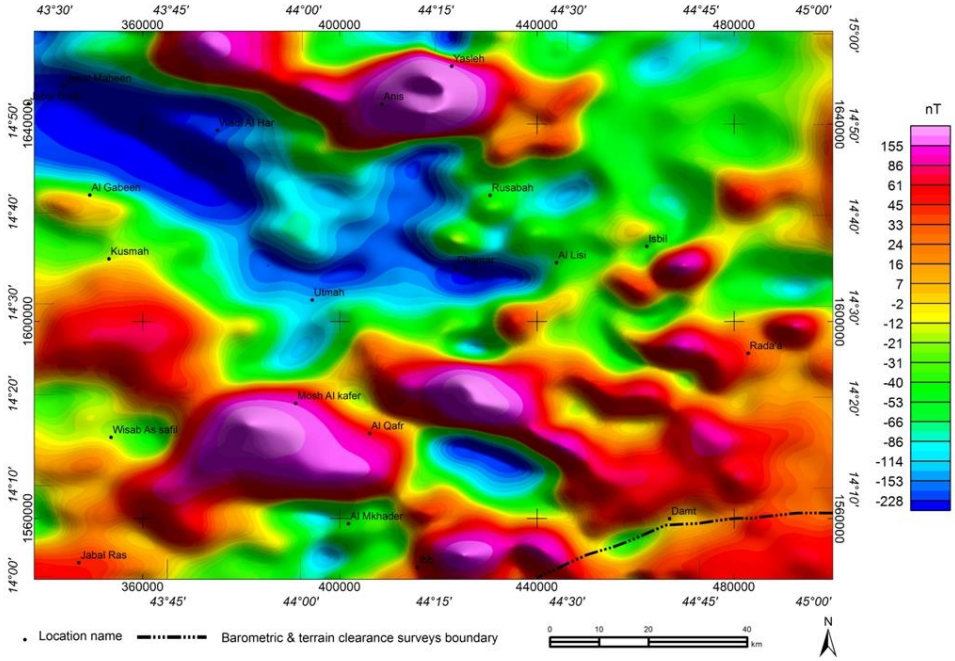

Fig. 3 Reduced to the pole aeromagnetic anomaly map (RTP) of the study area

EDGE DETECTOR TECHNIQUES

Mapping of lithological and structural contacts between the different rock units is a basic task in the geological interpretation of magnetic data. In this study, seven edge detector filters were used to delineate the contacts between magnetic anomalies. The theoretical principles of these techniques are briefly described below.

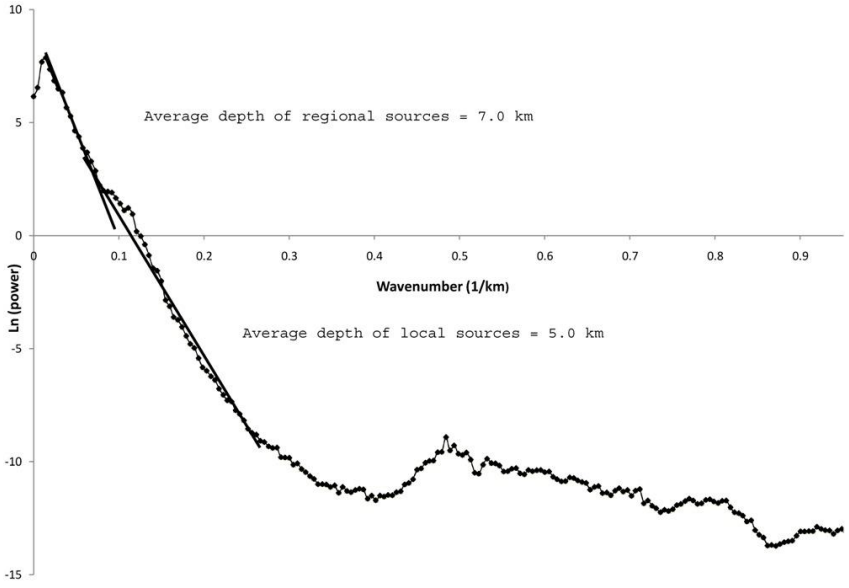

Fig. 4 2D radially averaged power spectrum of the RTP data of the study area

Vertical derivative (VDR)

The first vertical derivative filter is usually used to enhance and sharpen the edges of shallow anomalies, allowing clear delineation of vertical sources by tracing the zero contour (Ansari

and Alamdar 2011). This transformation defined as:

$$VDR = \partial T/\partial z \quad (1)$$

Where T is the total magnetic field and $\partial T/\partial Z$ is the vertical derivative of the magnetic field.

Total horizontal derivative (THD)

The THD is a commonly used edge detector filter given by Cordell and Grauch (1985) and defined as:

$$THD = \sqrt{\left(\frac{\partial T}{\partial x}\right)^2 + \left(\frac{\partial T}{\partial y}\right)^2} \quad (2)$$

Where $\partial T/\partial x$ and $\partial T/\partial y$ are the horizontal derivatives of the magnetic field in the x and y directions, respectively.

This function peaks over magnetic contacts under the next assumptions:

the magnetic field and source magnetization are vertical; the contact is vertical and isolated and the source is thick (Phillips 2000). This method detects well the edges of shallow bodies, but the deep sources are poorly imaged (Arisoy and Dikmen 2013).

Tilt angle derivative (TDR)

The tilt angle derivative filter (Miller and Singh, 1994; Verduzco et al. 2004), also called tilt angle or tilt derivative, is developed to locate the edges of magnetic anomaly sources without prior information on the source configuration by using the horizontal gradient amplitude of the tilt angle. It is defined as:

$$TDR = \tan^{-1}\left(\frac{\partial T/\partial z}{\sqrt{(\partial T/\partial x)^2+(\partial T/\partial y)^2}}\right) \quad (3)$$

The amplitude of the TDR ranges between ± π/2, positive values located directly above the source, negative values located far from the source and the zero contour traced the contact. This filter detects well the edges of shallow sources (Arisoy and Dikmen 2013).

Theta map

Theta map function is a normalization of the THD by the analytic signal filter and defined by Wijns et al. (2005) as:

$$\cos\theta = \left(\frac{\sqrt{(\partial T/\partial x)^2+(\partial T/\partial y)^2}}{\sqrt{(\partial T/\partial x)^2+(\partial T/\partial y)^2+(\partial T/\partial z)^2}}\right) \quad (4)$$

The theta function has a value restricted between 0 and 1 and peaks over the vertical contact, which coincides with the zero contours of the vertical derivative. This function delineates well the edges of shallow sources but the edges of deep sources are diffused (Ansari and Almdar 2013).

Horizontal tilt angle (TDX)

The TDX filter (Cooper and Cowan, 2006) is the normalization of the amplitude of the total horizontal derivative by the vertical derivative. The zero contour of this function coincides with the source edges.

$$TDX = \tan^{-1}\left(\frac{\sqrt{(\partial T/\partial x)^2+(\partial T/\partial y)^2}}{\partial T/\partial z}\right) \quad (5)$$

The angle defined by the TDX is restricted between ±π/2, similar to the tilt angle but it has a much sharper gradient over the contact (Fairhead and Williams 2006). This filter delineates well the edges of shallow and deep bodies (Arisoy and Dikmen 2013).

ETILT filter

The ETilt filter is defined as the ratio of the vertical derivative to the total horizontal derivative of the analytic signal (Arisoy and Dikmen 2013).

$$\mathrm{ETilt} = \tan^{-1}\left(\mathrm{k}\frac{\partial \mathrm{T}/\partial \mathrm{z}}{\sqrt{(\partial \mathrm{AS}/\partial \mathrm{x})^2+(\partial \mathrm{AS}/\partial \mathrm{y})^2}}\right) \quad (6)$$

Where $\mathrm{K} = 1/\sqrt{\Delta \mathrm{x}^2 + \Delta \mathrm{y}^2}$;

k is the dimensional correction factor, which does not affect the ETilt response, Δx and Δy are the sampling interval in the x and y directions, respectively.

The total horizontal derivative of the ETilt, termed as the enhanced total horizontal derivative of the tilt angle "ETHDR", is used as an edge detector (Arisoy and Dikmen 2013):

$$\mathrm{ETHDR} = \sqrt{(\partial \mathrm{ETilt}/\partial \mathrm{x})^2 + (\partial \mathrm{ETilt}/\partial \mathrm{y})^2} \quad (7)$$

This filter produces a very sharp gradient over the edges of both shallow and deep bodies, but it strongly amplifies noise in the data (Arisoy and Dikmen 2013).

Euler Deconvolution

This technique becomes a powerful tool for estimating the depth of magnetic sources and locating their edges. The advantages of this method include that it is independent of the direction of magnetization, no prior geologic model is required and not affected by the remanent field (Ravat 1996). Euler's homogeneity relation is given as:

$$\frac{\partial \mathrm{T}}{\partial \mathrm{x}}(\mathrm{x}-\mathrm{x_o}) + \frac{\partial \mathrm{T}}{\partial \mathrm{y}}(\mathrm{y}-\mathrm{y_o}) + \frac{\partial \mathrm{T}}{\partial \mathrm{z}}(\mathrm{z}-\mathrm{z_o}) = \mathrm{N}(\mathrm{B}-\mathrm{T}) \quad (8)$$

where: x_o, y_o and z_o are the coordinates of the source location whose total field (T) is measured at (x, y, z), B is the regional component of the total field and N is the degree of homogeneity, known as a structural index (SI) which describe the rate of the field change with distance. For magnetic data, the SI value ranges from 0 to 3 for various types of geological structures (Reid et al. 1990).

In this work, Euler deconvolution was applied to the RTP, regional and local data sets. A moving window with different size (ranging from 8 × 8 to 20 × 20 grid nodes) was tried and several SI values (0 - 3) were also tested and found that the SI values of 0 (for simple contacts /faults with a small depth-throw ratio and vertical dykes), and 1.0 (for dykes, sills and/or faults with a large depth-throw ratio).

RESULTS AND DISCUSSION

The RTP and regional anomaly sets subjected to the above mentioned edge detector filters and the results of these techniques from each set are incorporated to produce the integrated boundary maps which are superimposed over the magnetic anomaly maps of these data sets. Only boundaries confirmed at least by three techniques were involved in creating integrated boundaries. The next paragraphs are briefly described the general outline of the results obtained by edge detector filters.

For each data set, the zero contour of the VDR (which is tracing the horizontal extent of vertical sources) coincides exactly with the zero contours of the TDR, TDX and Etilt derivatives.

Peaks of the theta, TDX and ETHDR filters from regional anomalies are highly correlated and

tracking very well the zero contour of the VDR, nevertheless of the noise associated with the ETHDR results which is randomly distributed between the symmetrically arranged peaks over the source edges (i.e. not affected the accurate delineation of sources edges). On the other side, the THD peaks are not continuous and poorly correlated with the edges of deep sources.
Theta peaks from the RTP data tracking exactly the zero contour of the VDR. The maxima of TDX and ETHDR filters are also coincide with the zero contour of the VDR, despite the relatively intermediate and high noise level associated with the results of these filters, respectively, which is mostly located away from the source edges. As in the regional anomalies, the THD filter is poorly detected the RTP anomaly sources.
Optimum Euler solutions obtained from the RTP, regional and local anomaly sets are posted on magnetic anomaly maps of these sets, as shown below, while the depth range and the parameters of these solutions are listed in table (1).

Table 1 Optimum Euler solution from the different sets of magnetic anomalies

Data set name	Window size (grid nodes)	Structural index (SI)	Depth tolerance %	Depth range (km)
RTP	20 × 20	0	15	-0.33 – 7.3
		1	20	-0.23 – 5.7
Regional	20 × 20	0	15	-0.32 – 7.3
Local	12 × 12	1	3	-0.65 – 2.2
	10 × 10	0	15	1.7 – 4.6

In addition to the edge detector filters and Euler deconvolution, the RTP, regional and local anomaly groups are carefully analyzed in terms of the major tectonic events and lithology of the study area, as described in the following sections.

RTP magnetic anomalies

The RTP map and the superimposed integrated boundaries (Fig. 5a &b) shows that the dominant anomaly belts in the area trending E-W to WWN & EES, NW-SE and NE-SW and dissected by several major to sub-major faults with different trends, as shown by the in this figure. These trends are attributed to the reactivation of older Precambrian trends during the Mesozoic and Cenozoic associated, respectively, with the development of the major basins in Yemen and the separation of Arabia from Africa (Chiesa et al. 1983; Huchon et al. 1991).
The upper half of the area is dominated by a wide negative belt trending NW-SE, E-W and NE-SW in the western, middle and eastern parts, respectively. The western and northeastern parts of this belt correlated generally with a relatively low topography. On the geological map, this belt is mostly associated with Tertiary volcanics (YTS) in addition to the crystalline basement at the upper eastern corner of the area. The negative anomaly in such volcanic region can be attributed to reversely magnetized volcanic rocks, as indicated by Abou-Deeb et al. (2002), and also to wide subsurface hydrothermal alteration which is totally or partially disintegrated ferromagnetic minerals in volcanic rocks (Al Kadasi et al. 2020), while the variation of topography is responsible for the low amplitude (around 0 nT) values. The northern part of the area is mainly occupied by positive anomaly belt oriented WWN - EES. Only the two peaks of this belt are correlated with intrusive granite and associated with high

topography, indicating that the largest part of this anomaly source is buried. The short wavelength positive and negative anomalies to the south of the Isbil and Al Lisi active volcanoes are mostly referred to small horst - graben structures that characterized the Dhamar – Rada'a Quaternary volcanic field (Chiesa et al. 1983).

On contrary, the lower half of the area is dominated by positive anomaly belts oriented mostly NW – SE and separated by elongated negative anomaly closures. Positive anomalies in the western part of the area, which is generally of low topography, correlated at the surface with intrusive bodies of the YTS - mainly granite. The eastern part of the lower half of the RTP map is dominated by positive anomalies associated mostly with high topography and correlated with patches of the YTS intrusive bodies (gabbro) and the YVS basaltic lava scattered through these anomalies, indicating that large parts of these anomaly sources are not exposed.

The integrated boundaries of the RTP anomalies, the interpreted major to sub-major faults and Euler solutions of these anomalies are shown in figure (5a &b). This figure shows that the integrated boundaries enhanced several structural features which are not recognized clearly on the RTP map (Fig. 3).

Figure (5a) shows two types of Euler solutions, with depths varying from -0.33 to 7.26 km, are obtained from RTP anomalies with SI= 0. The linearly arranged solutions (often related to lithologic contacts, faults with small depth-throw ratio) are closely concentrated along the edges of magnetic anomalies and coincide exactly with the integrated boundaries obtained by the edge detector filters. While the rounded closures of Euler solutions are mostly correlated with magnetic anomalies of similar shape attributed to vertical dikes and plutons intruded the area, some of these anomalies correlated at the surface with YTS intrusive bodies.

On the other side, Euler solutions with SI= 1.0 (Fig. 5b) indicate that several dikes/ sills intruded the area at depths vary between -0.35 – 5.95 km concentrated in the eastern part faults below and around Dhamar – Rada'a Quaternary volcanic field, as well as below and around some of the YTS intrusive bodies.

Regional magnetic anomalies

Regional magnetic anomalies, along with the overlying integrated boundaries and the major to sub-major faults interpreted from this data set are shown in figure (6). This figure shows alternation of positive and negative anomaly belts trending mainly NW-SE, E-W, NE-SW and rarely N-S. These belts dissected by several faults oriented mostly NW-SE, NE-SW and NNW-SSE to N-S. This figure also shows that the traced boundaries of the WadiSiham – Ad Dali' basin from figure (2) are highly correlated with the obliquely extended magnetic anomalies between the western and southern limits of the area. This basin was originally formed during the Mesozoic, by rejuvenating the Najd fault system and its conjugate

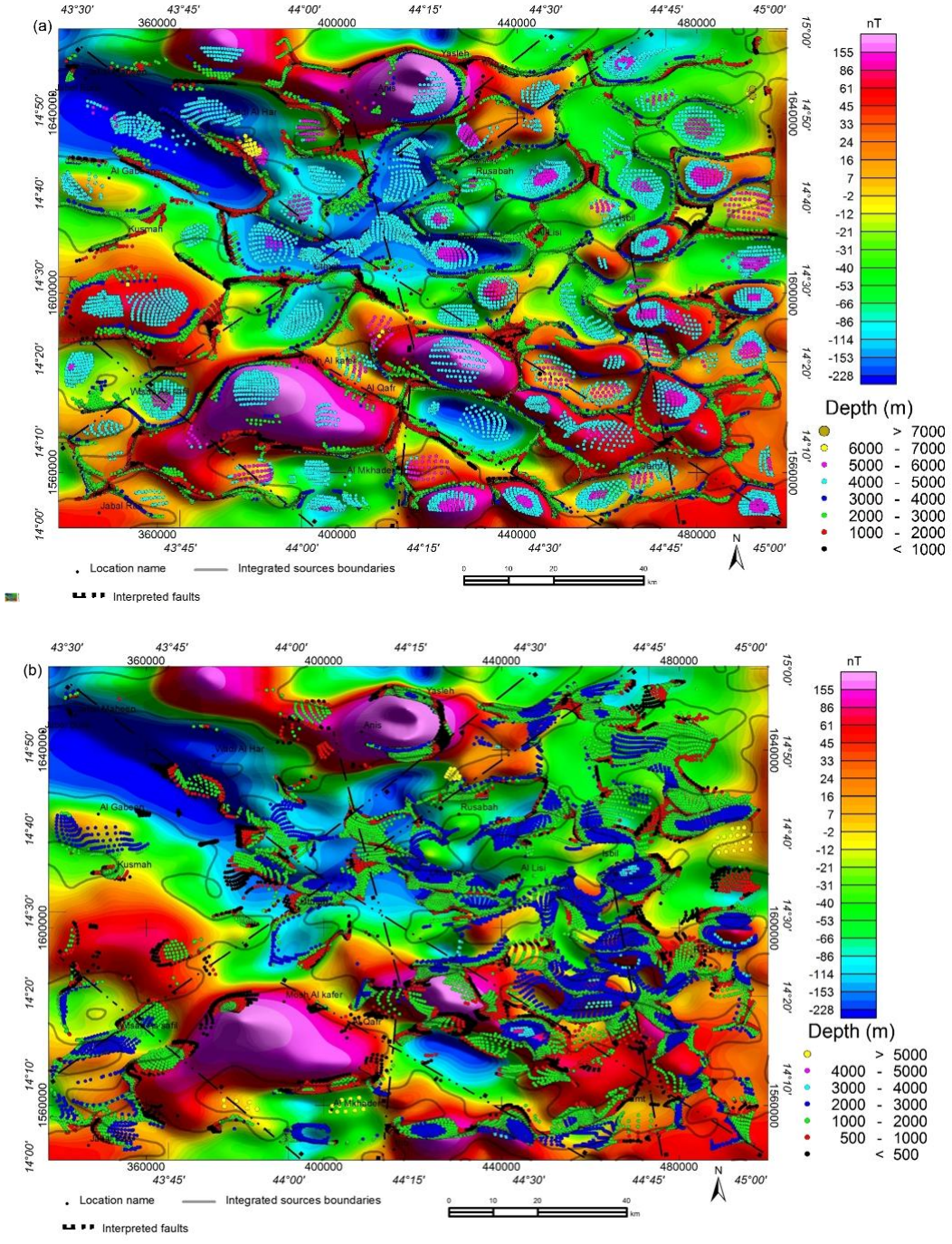

Fig. 5 RTP map superimposed by integrated boundaries and Euler solutions with (a) SI= 0 and (b) SI= 1

trends, and reactivated during the Oligo- Miocene where it is covered by a thick sequence of the YTS erupted through several of the reactivated and newly developed faults during this period of deformation.

In addition to the WadiSiham – Ad Dali' basin, two regional structural features were also traced from the map of sedimentary basins in Yemen. These features, not defined in the legend of this map but they are often referred to faults, match exactly the fault criteria on the

regional anomaly map (Fig. 6). The western one of these features is mostly related to listric fault extended through the study area, in the transitional zone between the Yemeni highlands and Tihamah plain, from north to south. While the eastern one correlates well with a fault-like structure at the northern part of the regional anomaly map and can be easily linked with a N-S trending fault evidence on this

map extended to the southern part of the area. The sedimentary basins map (Fig. 2) shows that the traced faults extended northward to the Paleozoic Sana'a basin, which suggests that this Paleozoic basin may be extended through the highlands (plateau), in the western part of Yemen, below the Cenozoic and Mesozoic lithologic units, from the north of Sana'a to the study area, at least. Analysis of aeromagnetic data of this region is required to confirm this assumption.

Despite of its small bandwidth (0.0145 – 0.070 km^{-1}), the regional magnetic anomaly map reflects anomalies with relatively intermediate wavelengths may be due to the higher magmatic activity affected the area during the Late Precambrian and Cenozoic time. To understand the complex geologic setting and tectonic development of the area, two anomaly sets with wave number bandwidths of 0.0145 – 0.030 km^{-1} and 0.0145 - 0.024 km^{-1} are extracted from the regional anomaly data and presented in figure (7a & b, respectively). This figure shows that the long-wavelength magnetic anomalies are well isolated. Moreover, the interpreted major to sub-major faults from figure (6) and the traced structures from the sedimentary basins map are exactly match the magnetic anomalies related to these features in the extracted maps (Fig. 7).

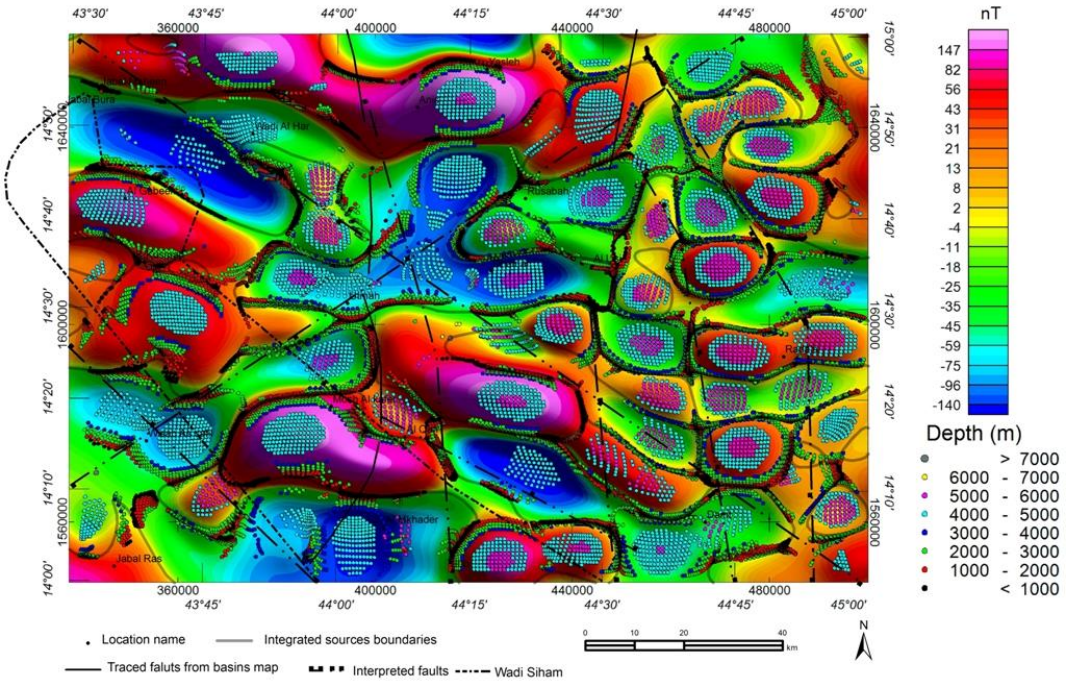

Fig. 6 Regional magnetic anomaly map of the study area superposed by integrated boundaries and Euler solutions with SI= 0

As shown in figures (6 and7) the western part of the area is mostly affected by NW-SE

trending shear during the last stage of the Pan African Orogeny, while the southern and eastern parts are dominated by NE-SW trending shear associated with a northward tilt increases eastward. Several normal faults also developed during this phase of deformation some of them with strike-slip component, which resulted in

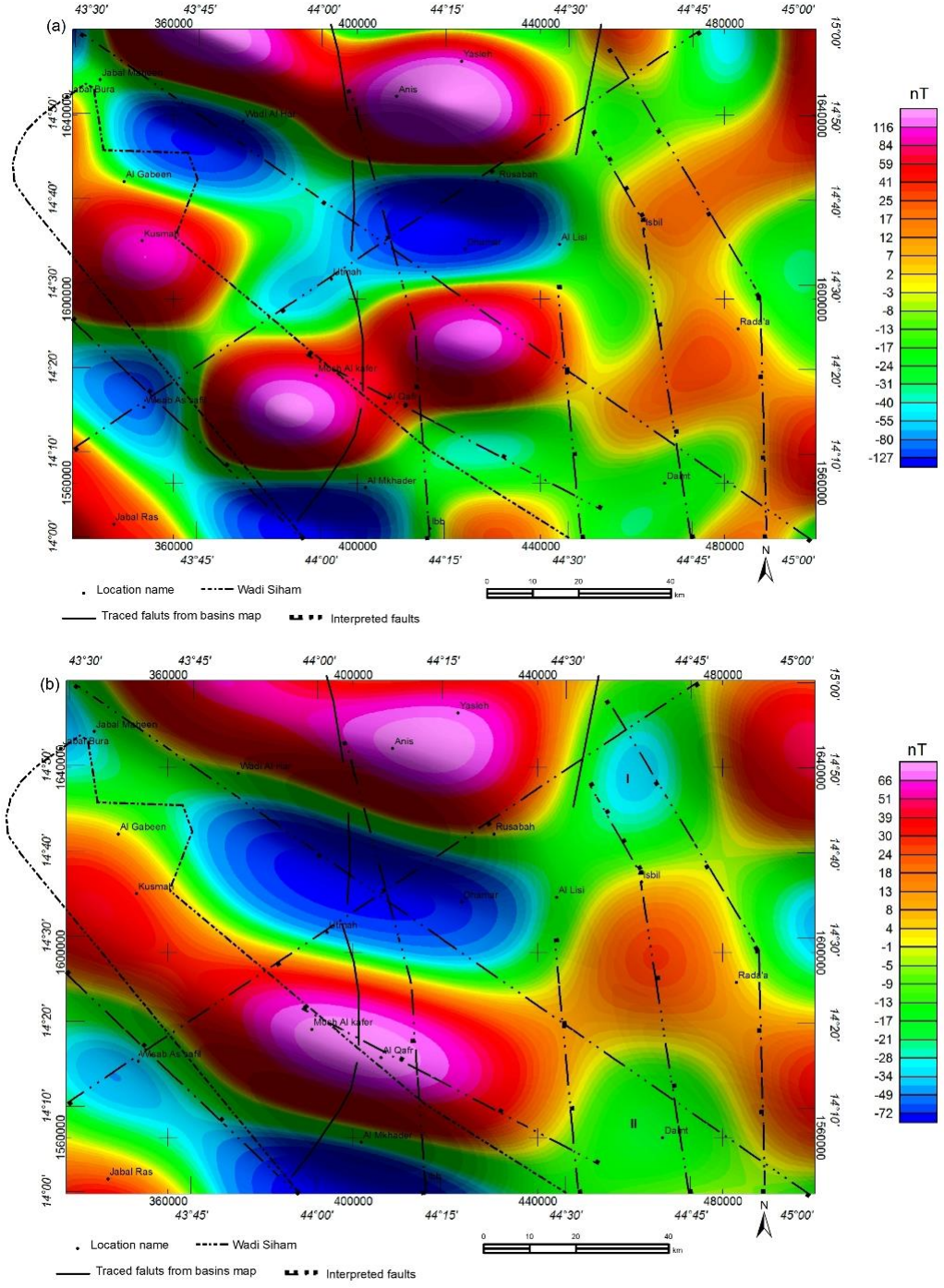

Fig. 7 Regional magnetic anomaly map of the study area extracted from figure (6) with wavenumber bandwidths of (a) 0.01452 - 0.030 km^{-1} and (b) 0.01452 - 0.0242 km^{-1}

small rotations of the tilted blocks (Figs. 6 and 7).

The orientation of the exposed basement rocks in the western and eastern parts of the area

(NW-SE and NE-SW, respectively Fig. 1) is consistent with the dominant anomaly trends in these parts (Figs. 6 & 7). Due to the absence of the basement exposures in the middle part of the area, the E-W trending magnetic anomalies in this part (Figs. 6 & 7) can be correlated with the E-W oriented basement block outcropped SE of Taiz town, about 55 km south of the study area.

The escape blocks tectonism associated the collision of east and west Gondwana during the last stage of the Pan African Orogeny resulted in the development of deep basins and other extensional structures which largely contributed to the wide intrusive activity affected the Arabian shield during this period.

In the study area, two narrow grabens (I & II) were developed by escape blocks tectonism in the eastern part of the area, beneath and around the Dhamar – Rada'a Quaternary volcanic field and the Damt geothermal site, (Fig. 7b) trending N-S and seem to terminate the NW-SE and E-W trending regional anomalies in the western and middle parts of the area (Fig. 7a &b). The western and eastern boundaries of these basins correlate to large extent, respectively, the limits of the volcanic plateau and basement at the surface.

The fumarole activity at the Al Lisi volcano in the Dhamar – Rada'a volcanic field and the highest mantle imprint of gasses emitted at the Damt geothermal site (compared with the other geothermal sites in Yemen, Minissale et al. 2007) can be attributed to these deeper structures. Furthermore, the N-S orientation of the Dhamar – Rada'a Quaternary volcanic field suggests that this period of volcanic activity is mostly originated by reactivating these deeper structures which permit the generation of magma feeding this activity by partial melting of hot mantle spots mapped in this region at about 72 km depth (Korostelev et al. 2014; Al Kadasi et al. 2020). The mantle traces recorded in this volcanic field by Manetti et al.(1991) support this hypothesis.

The relationship between the different structural trends affected the study area (Figs. 6 & 7) indicates that the area subjected to several periods of deformation but it is dominated by the fourth and sixth (final) phases, according to the classification of Precambrian deformations given by Heikal et al. (2013). The fourth phase characterized by normal faults trending NE-SW, and less frequently NW-SE and NNE-SSW, associated with local shear zones, graben and horst blocks. While the final phase of deformation is dominated by rifting, extrusion of alkaline plutons, volcanic rocks and ring complexes caused by extension related fold with fold axes trending EEN–WWS to E–W (Heikal et al. 2013).

As in the RTP anomalies, Euler solutions of regional magnetic anomalies with SI= 0 show linear and rounded-shaped solutions with depths ranged between -0.32 – 7.3 km. The linear solutions which are mostly referred to faults and/or contacts tracking the edges of magnetic anomalies and highly match the integrated boundaries (Fig. 6). The rounded Euler solution clusters are mostly concentrated above similarly shaped magnetic anomalies can be attributed to the late to post-tectonic plutons (e.g. metagabbro, diorite, granites, and syenites) and also to the roots of the ring complexes and new volcanics intruded the basement during the final phase of Precambrian deformation (Heikal et al. 2013).

A similar pattern of abundant E-W to NW-SE trending magnetic anomalies is observed by Nehlig et al. (2002) in the southern part of the Arabian shield connected at the surface with

late to post-tectonic circular, elongate, or raindrop-shaped felsic intrusions and mafic sills, dike swarms and ring dikes.

Due to the recur reactivation of Precambrian structural trends during the Cenozoic and in view of the very limited outcrops of the late to post-tectonic plutons in the study area, the rounded-shaped Euler solutions may also be related to the conduits (pathways) feeding the intensive Cenozoic volcanic and intrusive activities by magma.

Local magnetic anomalies

Figure (8) is more crowded by alternating positive and negative anomaly belts trending mainly E-W, EEN, WWN, NW & NE and rarely N-S referred to rock bodies intruded the study area, as a part of the volcanic plateau, during the second phase of the YTS volcanic activity and to some extent during the Quaternary volcanic activity. These belts are highly dissected by several faults, mostly normal faults, trending mainly NNW-SSE to NW-SE, NNE-SSW to NE-SW and N-S. The NW-SE and NE-SW trending regional magnetic anomalies observed on figures (6 & 7) can be also traced on the local anomaly map (Fig. 8) by linking the isolated fault criteria. Such correlation indicates the recent reactivation of these regional trends.

Euler solutions of local magnetic anomalies with SI= 0, referred to faults and/or contacts, are tightly clustered along the edges of anomaly sources which are located at depths ranged between 1.7 – 4.6 km (Fig. 8a). On the other hand, Euler solutions obtained with SI= 1.0 are mostly concentrated over the anomaly belts (Fig. 8b) and reflect that the area is heavily intruded by dikes/sills at depths ranged between - 0.65 – 2.2 km, associated with the second phase of the YTS and to some extent with the YVS.

The widespread intrusions in the study area reflected by magnetic anomalies and Euler solutions can be attributed to the repeated rejuvenation of Precambrian faults during the Mesozoic and Cenozoic times which dissected the crust at different depths and forming nets of interconnected faults. These faults along with the abundant magma below the volcanic plateau, as indicated by earlier studies (e.g. Ahmed et al. 2013; Corbeau et al. 2014; Korostelev et al. 2014), provide suitable conditions for such intensive intrusion. A similar situation is found below the Afar depression where Hammond et al. (2011) recorded widespread melt in the lower crust and argued that magma intrusion has been active in the region over the last 30 Ma.

Structural framework of the study area

The gross structural pattern of the study area shown in figure (9) is deduced from the integrated boundary maps of the RTP and regional anomalies (Figs. 5 & 6) along with the interpreted major to sub-major faults from these anomaly sets. The upper half of the study area is mostly occupied by a large basin covered mainly by volcanic rocks in addition to the crystalline basement at the upper eastern corner. The relatively small size anomalies shown in this basin (Figs 5 and 6) are attributed to small-scale structural deformations and/or magmatic activity occurred during the last phase of Precambrian deformation and later. The interpreted faults from the regional and RTP magnetic anomaly maps (Figs 5 and 6) are identical to a great extent. Nearly all of these faults can be easily traced on the local anomaly map (Fig. 10) and most of them can be extended to new regions in the study area, based on the fault criteria indicated by local anomalies. Furthermore, most of these faults correlated well with the

mapped geologic faults, as shown in figure (10). This figure also shows that the boundaries of the large basin in the upper part of the area (Fig. 9) are highly tracked the boundary of local anomalies. These evidences confirm that the structural pattern of the study area is largely controlled by earlier tectonic events, mostly associated with the Pan African Orogeny phase of Precambrian deformation and later. The lower half of the area is dominated by several faults, small horst-graben structures formed by uplifted/thrusted blocks and intrusive bodies.

Among the regional faults interpreted from the regional anomaly map, the fault A-A' (Fig. 9) marks nearly the transitional zone between the Yemeni highlands and the Red Sea coastal plain (Tihamah plain), while the fault B-B' terminate the crystalline basement in the eastern part.

The higher correlation between the fault criteria on the local anomaly map and the mapped geological faults (Fig. 10) indicates that carefully isolated near-surface magnetic anomalies can be successfully used to extrapolate totally or partially buried faults and to confirm or adjust the path of inferred geological faults.

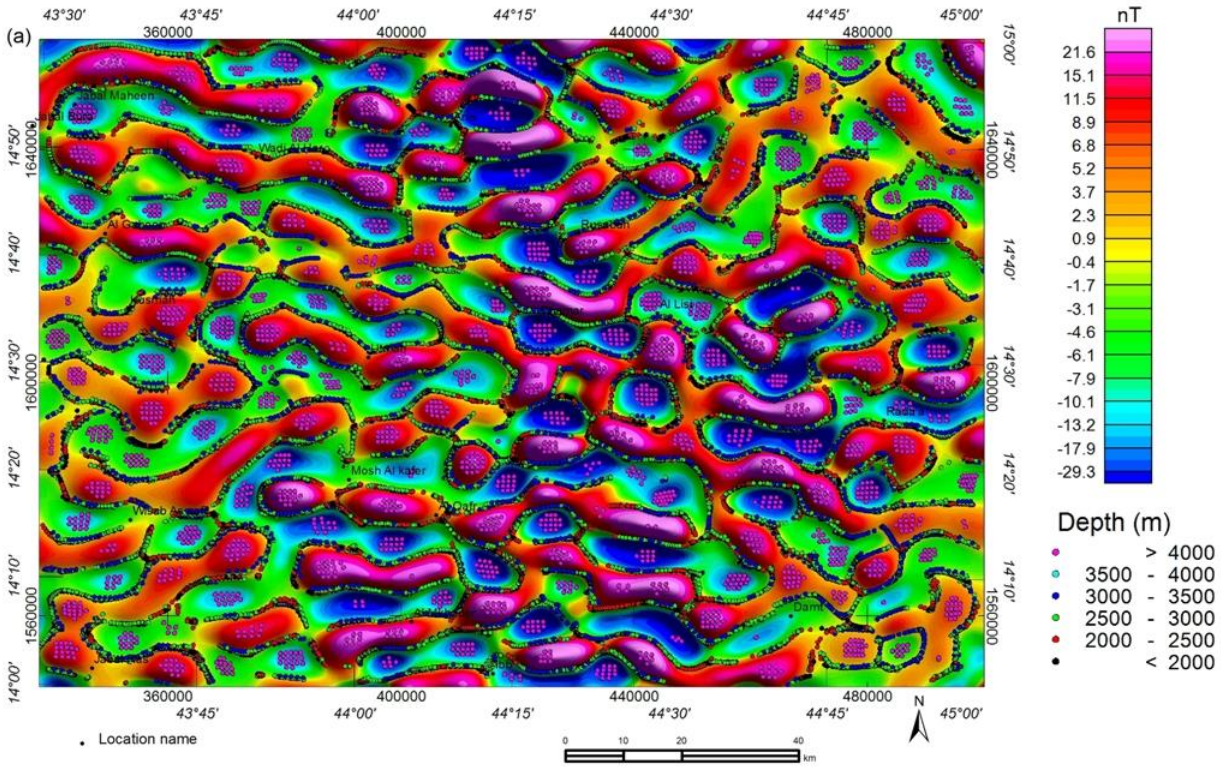

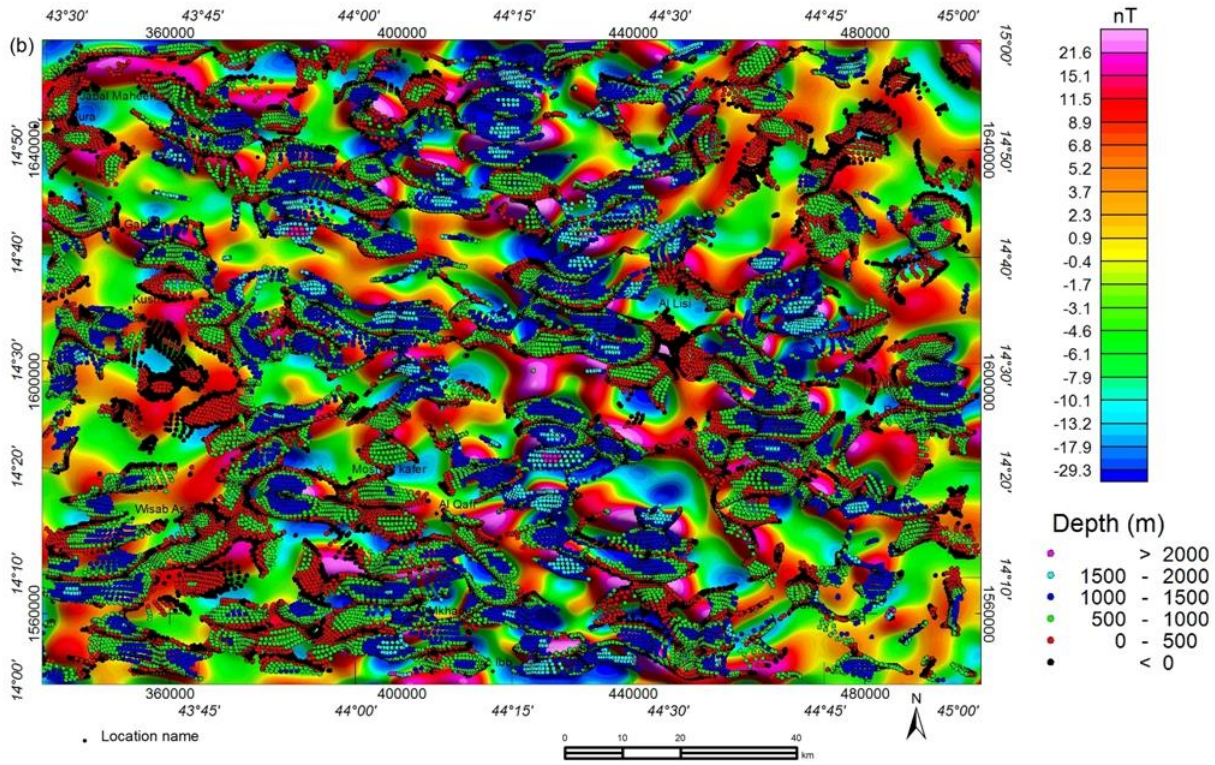

Fig. 8 Local magnetic anomaly map superposed by Euler solutions with (a) SI= 0 and (b)SI= 1

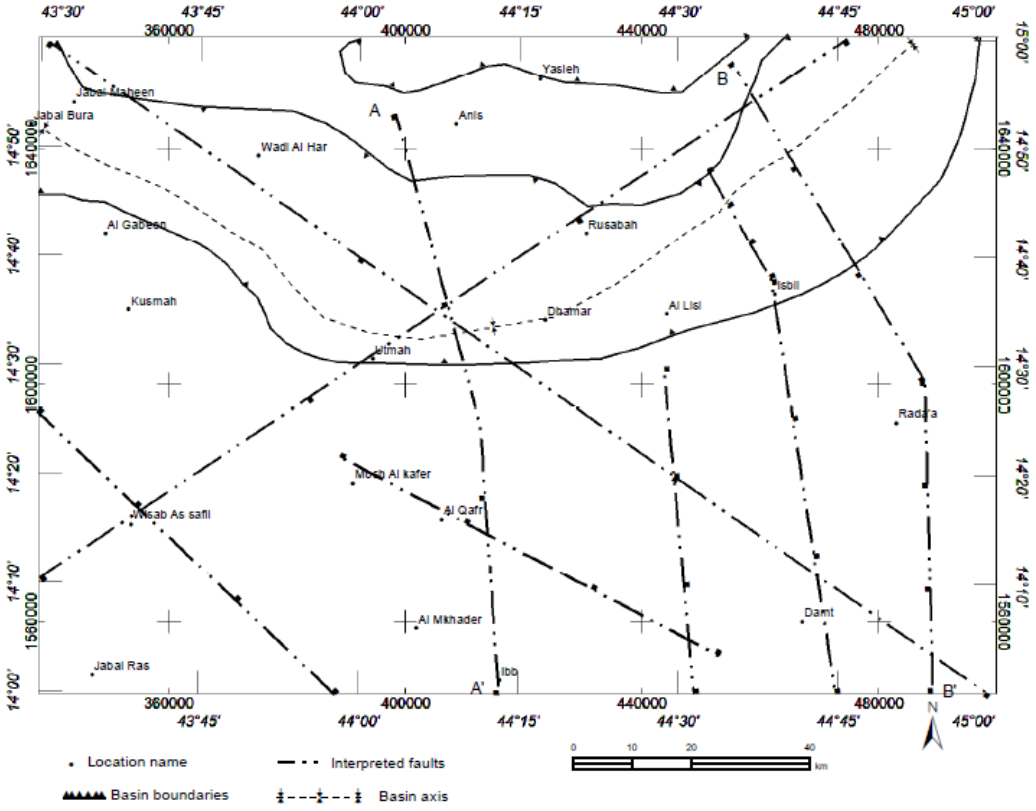

Fig. 9 Gross structural pattern of the study area deduced from the interpreted major

faults and integrated boundaries of the RTP and regional anomalies

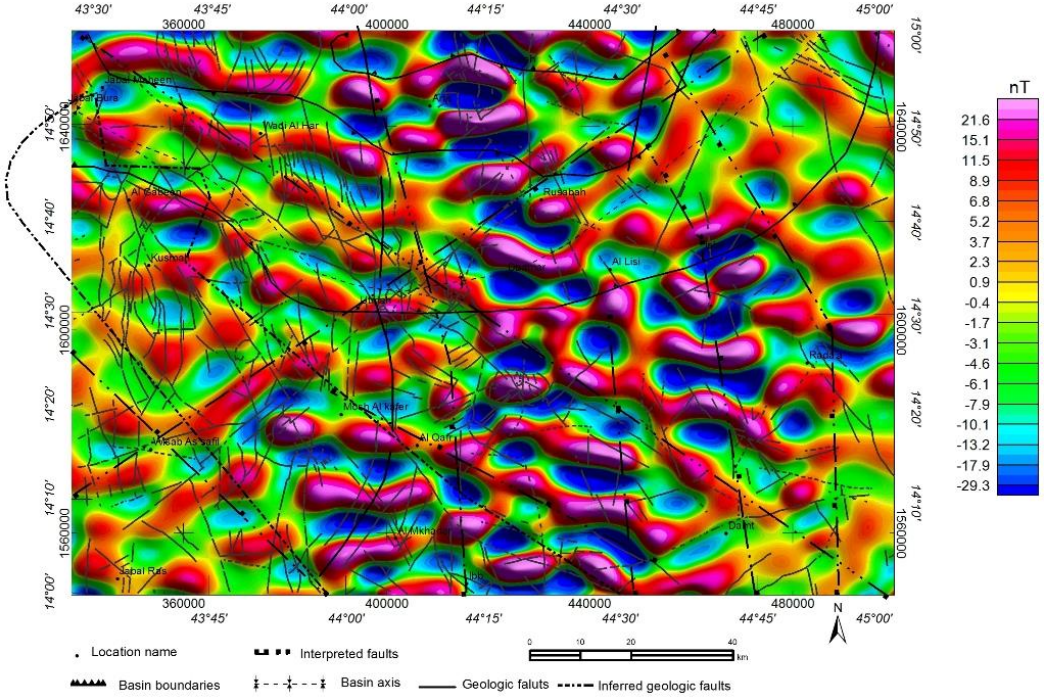

Fig. 10 Local magnetic anomaly map superposed by the linear geological structures and the gross structural pattern map of the area.

CONCLUSIONS

Based on the above discussion the following can be concluded:

- The Quaternary volcanic activity in the Dhamar – Rada'a volcanic field, the fumaroles at the Al Lisi volcano in this volcanic field, and the highest mantle impact of gasses emitted at the Damt geothermal field (compared with other geothermal fields in Yemen) are attributed to the reactivation of the N-S trending narrow grabens and other extensional structures developed beneath these fields during the final phase of the Pan African Orogeny.
- Integration of regional geologic faults from the sedimentary basins map and the interpreted faults from magnetic anomalies suggests that the Paleozoic Sana'a basin is extended through the western part of Yemen, beneath the Mesozoic and Cenozoic lithologies, to the study area.
- The THD filter is inefficient in mapping both deep and RTP anomaly sources. The results of the other used filters from each data set are highly correlated and well defined sources boundaries, despite the noise associated with some filters, which is randomly distributed between the systematically arranged edges.

ACKNOWLEDGMENT

Deep thanks to the Yemen geological survey and mineral resources board (YGSMRB) for providing the aeromagnetic data of the study area. The author is also grateful to Prof. Dr. Mahmoud M. Senosy for helpful comments on the draft version of this paper.

REFERENCES

Abou-Deeb JM., Tarling DH, Abdeldayem AL (2002) Preliminary paleomagnetic stratigraphy

of the tertiary Yemen Volcanics. Geofísica International 41: 37–47.

Ahmed A, Tiberi C, Leroy S, Stuart GW, Keir D, Sholan J, Khanbari K, Al-Ganad I, Basuyau C (2013) Crustal structure of the rifted volcanic margins and uplifted plateau of Western Yemen from receiver function analysis. Geophysical Journal International 193: 1673–1690.

Al Kadasi AN, Al-Aydrus A, Mustafa MS (2020) Estimation of Curie point depth in southwestern Yemen from spectral analysis of aeromagnetic data. Arabian Journal of Geosciences, https://doi.org/10.1007/s12517-020-5196-0

Ansari AH, Alamdar K (2011) A new edge detection method based on the analytic signal of tilt angle (ASTA) for magnetic and gravity anomalies. Iranian Journal of Science and Technology A2: 81 – 88.

Arisoy MO, Dikme, O (2013) Edge Detection of Magnetic Sources Using Enhanced Total Horizontal Derivative of the Tilt Angle. Yerbilimleri 34: 73-82.

As-Saruri M, Sorkhabi R, Baraba R (2010) Sedimentary basins of Yemen: their tectonic development and lithostratigraphic cover. Arabian Journal of Geosciences 3: 515–527. doi:10.1007/s12517-010-0189-z

Beydoun ZR, As-Saruri M, Baraba' RS (1996) Sedimentary basins of the Republic of Yemen: their structural evolution and geological characteristics. Revue de l'lnstit. Franfais du Petrole 51: 763–775, Paris.

Beydoun ZR, As-Saruri M, El-Nakhal H, Al-Ganad IN, Baraba' RS, Nani AO, Al-Aawah MH (1998) International Lexicon of Stratigraphy Republic of Yemen. Vol. III, Asia Fascicule 10b2, IUGS publication No. 34.

Blasband B, White S, Brooijmans P, De Boorder H ,Visser W (2000) Late Proterozoic extensional collapse in the Arabian-Nubian shield. Journal of the Geological Society 157: 615–628.

Chiesa S, La Volpe L, Lirer L, Orsi G (1983) Geological and structural outline of Yemen Plateau, Yemen Arab Republic. NeuesJahrbuch fur Geologie und Palaontolgie 11: 641-656.

Cooper GR, Cowan DR (2006) Enhancing potential field data using filters based on the local phase. Computer and Geosciences 32: 1585-1591.

Cooper GR, Cowan DR (2008) Edge enhancement of potential-field data using normalized statistics. Geophysics 73: H1–H4.

Cooper GR (2009) Balancing images of potential-field data. Geophysics 74: L17-L20.

Corbeau J, Rolandone F, Leory S, Al-Lazki A, Stork AL, Kier D, Stuart GW, Hammond JO, Doubre C, Vergne J, Ahmed A, Khanbari K (2014) Uppermost mantle velocity from Pn tomography in the Gulf of Aden. Geosphere. https://doi.org/10.1130/GES01052.1

Cordell L, Grauch V (1985) Mapping basement magnetization zones from aeromagnetic data in the San Juan Basin, New Mexico, In: Hinze, W., (Ed.), Utility of regional gravity and magnetic maps. Society of Exploration Geophysics 181–197.

Davison I, Al-Kadasi M, Al-Khirbash S, Al-Subbary AK, Baker J, Blakey S, Bosence D, Dart C, Heaton R, McClay K, Menzies M, Nicols G, Owen L, Yelland A (1994) Geological evolution of the southeastern Red Sea Rift margin, Republic of Yemen. Geological Society of America Bulletin 106:1474–1493.

Fairhead JD, Williams SE (2006) Evaluating Normalized Magnetic Derivatives for Structural Mapping, SEG 2006 New Orleans annual Meeting, Extended Abstract.

Hammond JOS, Kendall JM, Stuart GW, Keir D, Ebinger C, Ayele A, Belachew M (2011) The nature of the crust beneath the Afar triple junction: Evidence from receiver functions. Geochemistry Geophysics Geosystems 12: Q12004, doi:10.1029/2011GC003738.

Heikal M Th S, Al-Khirbash SA, Hassan AM, Al-Kotbah AH, Al-Selwi KM (2013) Lithostratigraphy, deformation history, and tectonic evolution of the basement rocks, Republic of Yemen: an overview, Arabian Journal of Geosciences DOI 10.1007/s12517-013-0951-0.

Huchon,P, Jestin F, Cantagrel JM, Gaulier JM, Al-Khirbash S, Gafaneh A (1991) Extensional deformations in Yemen since Oligocene and the Afar triple junction. AnnalesTectonicae 5: 141–163.

Korostelev F, Basuyau C, Leroy S, Tiber C, Ahmed A, Stuartm GW, Keir D, Rolandone F, Al Ganad I, Khanbari K, Boschi L (2014) Crustal and upper mantle structure beneath south-western margin of the Arabian Peninsula from teleseismic tomography. Geochemistry Geophysics Geosystems https://doi.org/10.1002/2014GC005316

Levin G, Park J (2000) Shear zones in the Proterozoic lithosphere of the Arabian Shield and the nature of the Hales discontinuity. Tectonophysics 323: 131–148.

Ma G, Liu C, Li L (2014) Balanced horizontal derivative of potential field data to recognize the edges and estimate location parameters of the source. Journal of Applied Geophysics 108: 2–18.

Manetti P, Capaldi G, Chiesa S, Civetta L, Conticelli S, Gasparon M, Volpe L, Orsi G (1991) Magmatismof the eastern Red Sea margin in the northern part of Yemen from Oligocene to present. Tectonophysics 198: 181–202.

Miller HG, Singh V (1994) Potential field tilt a new concept for location of potential field sources. Journal of Applied Geophysics 32: 213-217.

Minissale A, Mattash MA, Vaselli O, Tassi F, Al-Ganad IN, Selmo E, Shawki NM, Tedesco D, Poreda R, Ad-Dukhain AM, Hazzae MK (2007) Thermal springs, fumaroles and gas vents of continental Yemen: their relation with active tectonics, regional hydrology and the country's geothermal potential. Applied Geochemistry 22: 799–820.

Moseley F (1969) The Aden Traps of Dahla, Musaymir and Radfan, South Yemen. Bulletin Volcanologique., 33, 889-909.

Nehlig P, Genna A, Asfirane F (2002) A review of the Pan-African evolution of the Arabian Shield. GeoArabia, 7: 103–124.

Phillips J (2000) Locating magnetic contacts: A comparison of the horizontal gradient, analytic signal, and local wavenumber methods: 70th Annual International Meeting, Society of Exploration Geophysics, Expanded Abstracts 402–405.

Pilkington M, Keating P (2004) Contact mapping from gridded magnetic data – a comparison of techniques. Exploration Geophysics 35: 306–311.

Ravat D (1996) Analysis of the Euler method and its applicability in environmental magnetic investigations. Journal of Environmental and Engineering Geophysics 1: 229–238.

Reid AB, Allsop JM, Granser H, Millet AJ, Somerton IW (1990) Magnetic interpretation in

three dimensions using Euler deconvolution. Geophysics 55: 80-91.

Robertson PLC Group (1991) Magnetic anomaly map of Yemen.

Robertson PLC Group (1990) Geological map of Yemen, Dhamar (sheet 14G).

Stoeser DB, Camp VE (1985) Pan-African micro plate accretion of the Arabian shield. Geological Society of America Bulletin 96: 817–826.

Verduzco B, Fairhead JD, Green CM (2004) New insights into magnetic derivatives for structural mapping. The Leading Edge 23: 116-119.

Wijns C, Perez C, Kowalczyk P (2005) Theta Map: Edge detection in magnetic data. Geophysics 70: L39–L43.